Supporting material

Synergistic Strategy of Interfacial Ion Channels and Cross-linked Network in Composite Electrolyte for Dendrite-Free Sodium-Metal Batteries

Lei Zhai[a], Hanghang Dong[b], Haichao Wang[c], Yijie Duan[a], Zuo Liu[a], Shuang Yan[a], Chenguang You[a], Hao Yan[c], Xin Tan[a], Shuangqiang Chen[c, d, *]

a College of Chemistry and Materials Engineering, Wenzhou University, Wenzhou, Zhejiang 325035, China.

b. School of Energy and Power Engineering, Nanjing University of Science and Technology, Nanjing, 210094, China.

c State Key Laboratory of Advanced Fiber Materials, College of Materials Science and Engineering, Donghua University, Shanghai 201620, China

d Department of Chemical Engineering, School of Environmental and Chemical Engineering, Shanghai University, Shangda Road 99, Shanghai 200444, China.

Email: chensq@dhu.edu.cn (S. Chen)

Experimental section

Preparation of NZSPO

The crystal of $Na_3Zr_2Si_2PO_{12}$ (NZSPO) was synthesized *via* a conventional solid-state reaction. Stoichiometric precursors (Na_2CO_3, ZrO_2, SiO_2, and $NH_4H_2PO_4$) were thoroughly mixed by ball-milling at 400

rpm for 12 h. The mixture was subsequently pre-calcined at 900°C for 6 h, followed by second ball-milling step and final sintering at 1200°C for 12 h in air [18]. The phase purity of the as-obtained product was confirmed by X-ray diffraction (XRD).

Preparation of PPD-0 and PPD-x electrolytes

PPD-0: 1.0 g of PAN was dissolved in 8.0 g of N,N-Dimethylformamide (DMF) under stirring at 45°C for 2 h. Subsequently, 0.7 g of poly(ethylene glycol) diglycidyl ether (PEGDE) and 0.3 g of Polyoxybpropylenediamine (Mw. = ca.2000) (PD) were added in that solution, and then the solution was stirred at 55°C for 12 h to enable ring-opening polymerization. The slurry was cast onto a polytetrafluoroethylene plate and dried at 70°C for 12 h to form freestanding PPD-0 films. The thermal gravimetric test confirmed that DMF had completely evaporated under these conditions, leaving no residual DMF that would affect the properties of the polymer (Fig. S1).

PPD-x: a certain amount of NZSPO powder (x= 5, 10, 15 and 20 wt.%) was dispersed in the initial DMF solution via ultrasonication for 0.5 h prior to polymerization. The remaining steps were identical to those for PPD-0.

Materials characterization

The morphology of the as-prepared materials was characterized by scanning electron microscopy (SEM, Xplore-30). X-ray diffraction (XRD)

patterns were collected on a Rigaku Aeris diffractometer (Panalytical) using Cu-Kα radiation. Chemical structures were analyzed by Fourier-transform infrared (FT-IR) spectroscopy (Shimadzu, IRAffinity-1S). The surface chemical composition was determined by X-ray photoelectron spectroscopy (XPS, Thermo Scientific ESCALAB 250XI).

Electrochemical Measurements

Electrochemical impedance spectroscopy (EIS) was performed on a CHI760E electrochemical workstation over a frequency range of 0.1 Hz to 1 MHz with a 10 mV amplitude, using a blocking cell (stainless steel | electrolyte | stainless steel). The bulk (R_b) and interfacial (R_{int}) resistances were extracted from the corresponding Nyquist plots. The electrochemical stability window was evaluated by linear sweep voltammetry (LSV) at a scan rate of 1 mV s^{-1} from 2.0 to 5.0 V (vs. Na^+/Na) in a Na | electrolyte | stainless steel configuration. The Na^+ transference number (t_{Na^+}) was determined by combining potentiostatic polarization (10 mV DC bias) with EIS measurement in a Na | electrolyte | Na symmetric cell, using the equation:

$$t^+ = \frac{I_{ss}(\Delta V - I_0 R_0)}{I_0(\Delta V - I_{ss} R_{ss})}$$

Where I_0 and I_{ss} are the initial and steady-state currents, and R_o and R_{ss} are the corresponding interfacial resistances before and after polarization.

Cell Assembly and Testing

Symmetric Na cells (Na | solid electrolyte | Na) were assembled for transference number measurement and long-term cycling tests. For full cell tests, the cathode slurry was prepared by mixing $Na_3V_2(PO_4)_3$ (NVP), carbon black, and poly(vinylidene fluoride) (PVDF) binder in a weight ratio of 7:2:1, which was then coated onto an aluminum foil current collector and dried at 80 °C under vacuum. All cells were assembled in an Ar-filled glovebox (H_2O and O_2 levels < 0.1 ppm). For the NVP//Na full cells, 10 μL of electrolyte (PPD-10 or PPD-0) was used, with sodium metal as the anode. The galvanostatic charge-discharge tests were conducted within a voltage window of 2.5–3.8 V (vs. Na^+/Na) at 25 °C, and the mass loading of the active material (NVP) was controlled at 1.5–2.0 mg cm^{-2}.

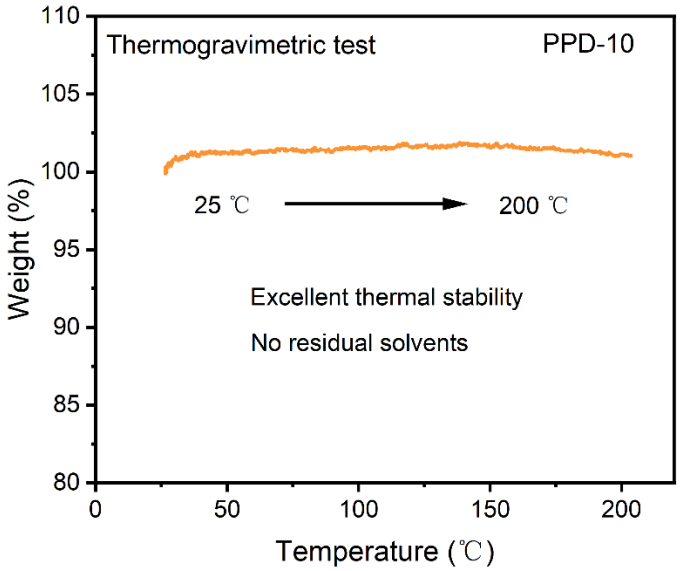

Fig. S1 Thermogravimetric curve of PPD-10 material at temperatures ranging from 25 to 200 degrees Celsius.

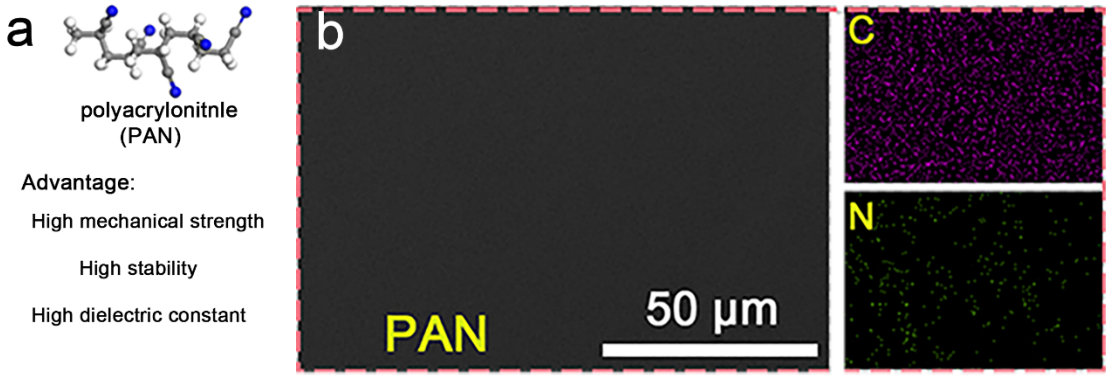

Fig. S2 a) Molecular structure of PAN; b) Scanning electron microscope images and elemental mapping of PAN.

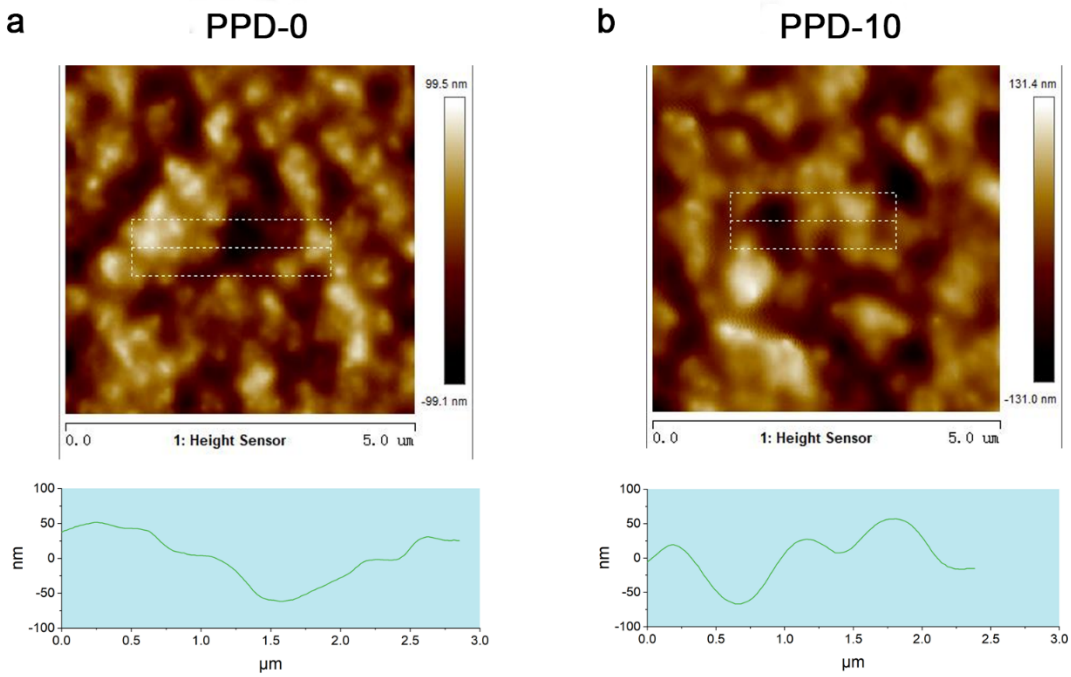

Fig. S3 AFM images of a) PPD-0 and b) PPD-10 with the thickness feature and height curves with the same test condition.

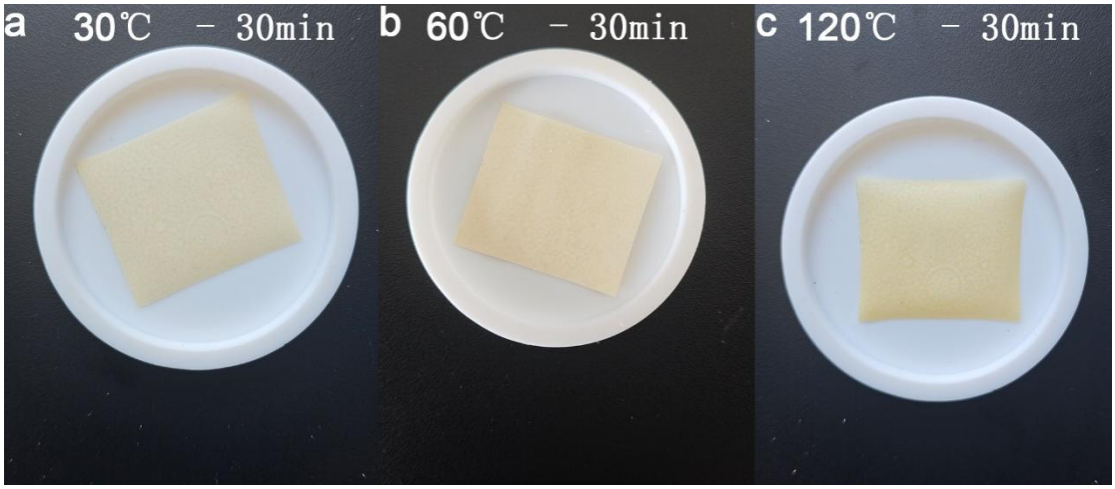

Fig. S4 High-temperature stability test of PPD-10 electrolyte: a) Store at 30℃ for 30 minutes; b) Store at 60℃ for 30 minutes; c) Store at 120℃ for 30 minutes.

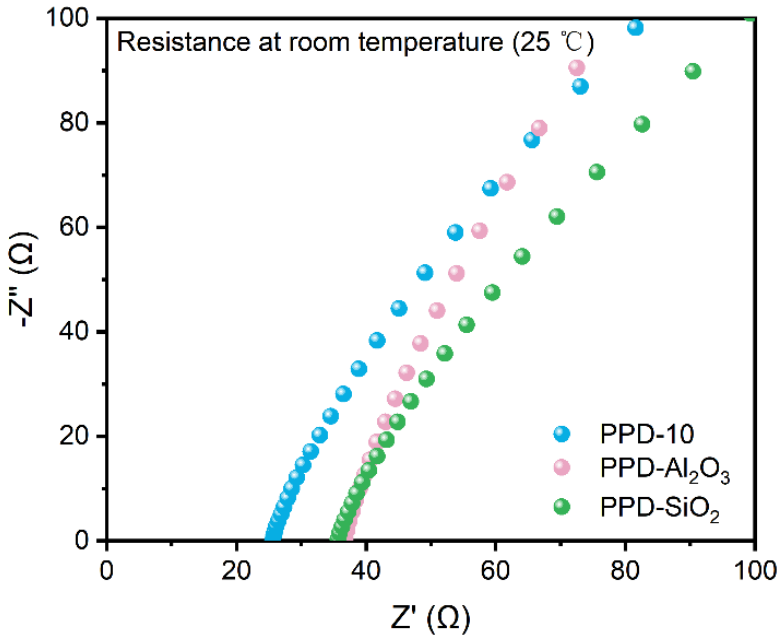

Fig. S5 Electrical conductivity tests of composite solid-state electrolytes prepared by adding different fillers (NZSPO, Al_2O_3, SiO_2) to PPD materials.

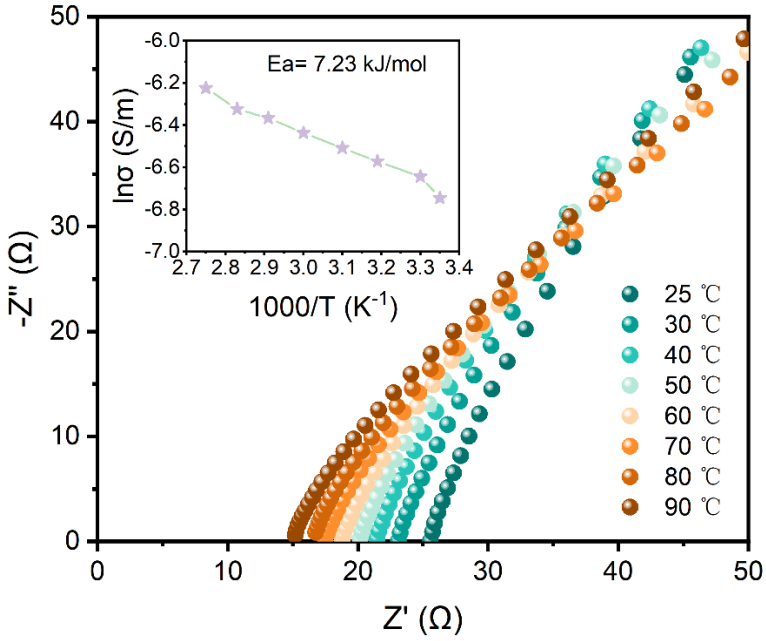

Fig. S6 Impedance testing of PPD-10 composite solid-state electrolyte material under temperature gradient, Arrhenius plots and corresponding activation energy.

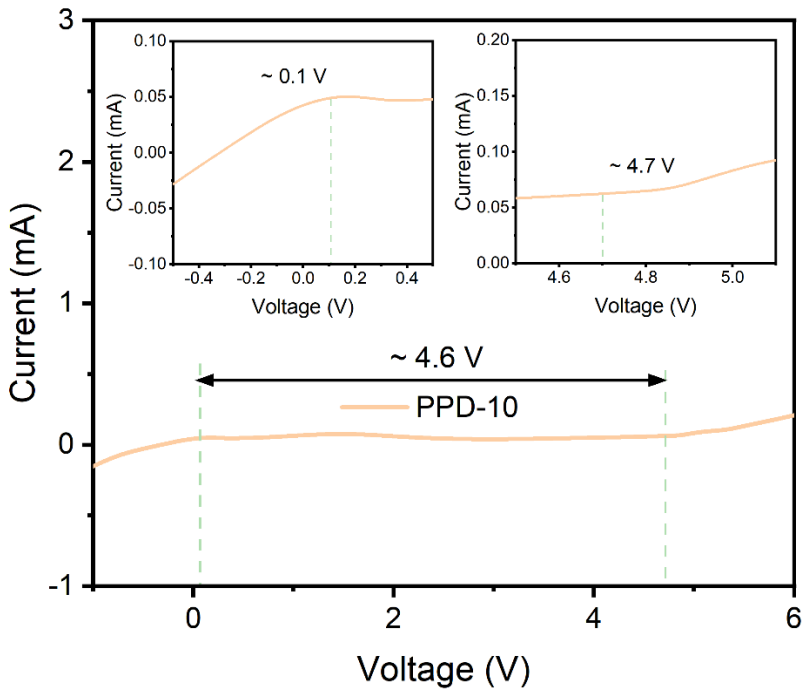

Fig. S7 Determination of the electrochemical window of PPD-10 material.

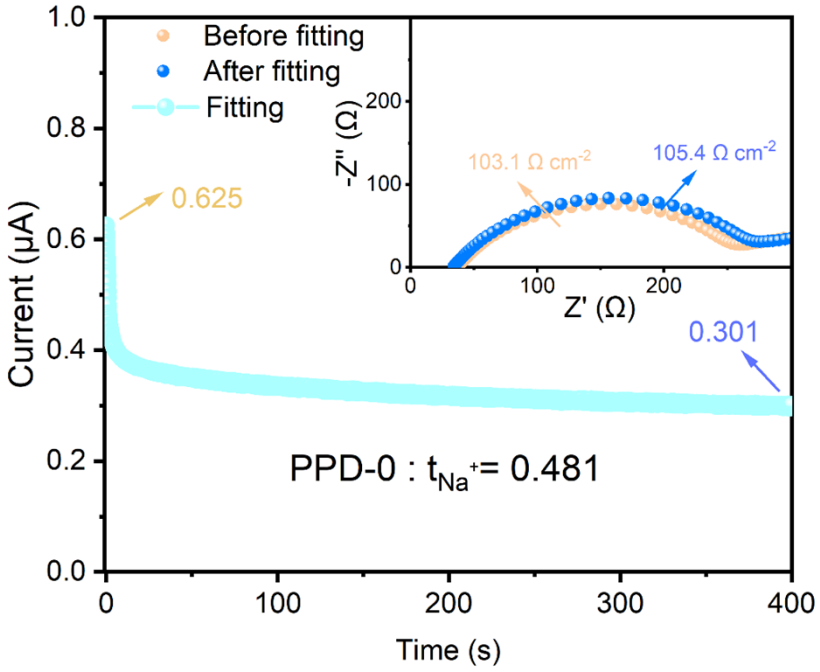

Fig. S8 DC polarization result for Na | PPD-0 | Na symmetrical battery at 10 mV s^{-1} and electrochemical impedance spectroscopy (EIS) variation (inset in plots) before and after polarization.

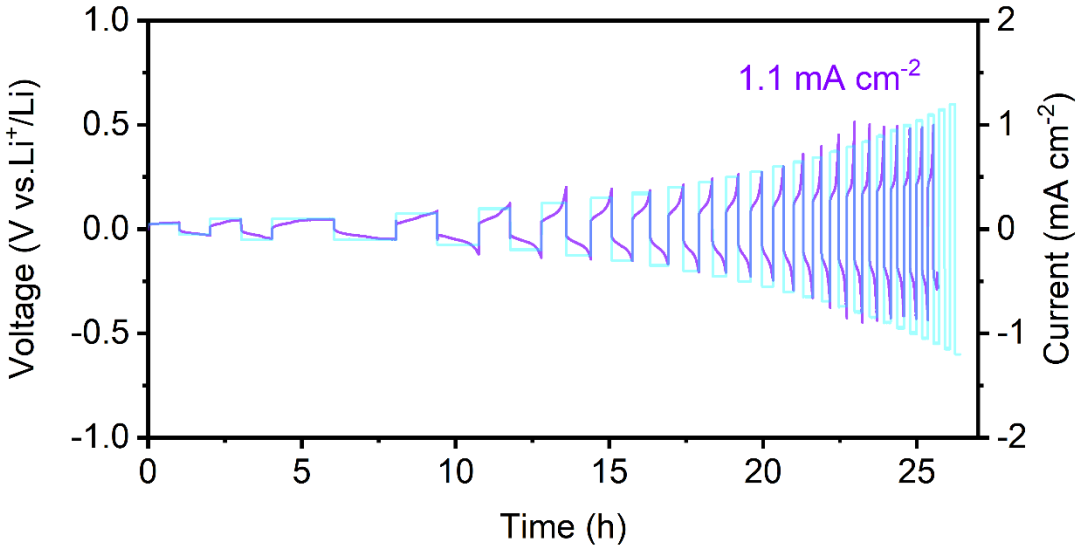

Fig. S9 Critical current density (CCD) tests of Na | PPD-0 | Na symmetric cells.

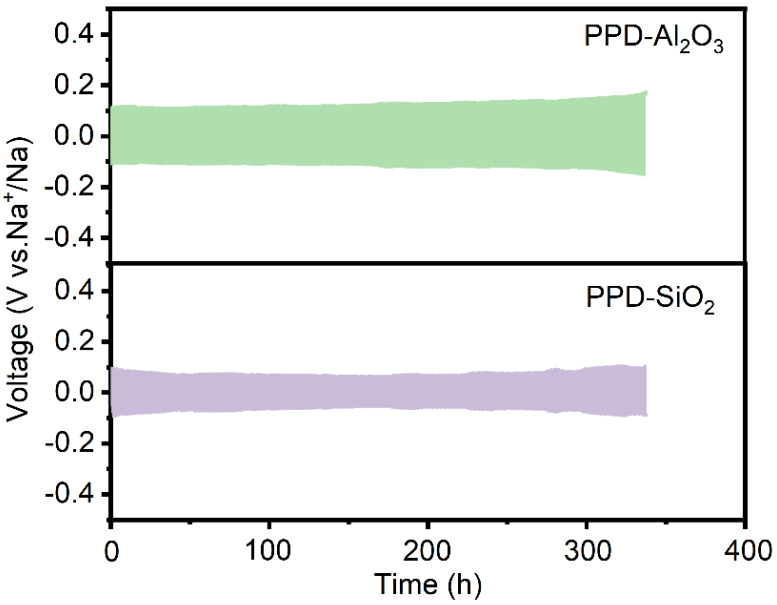

Fig. S10 Tests were conducted on symmetrical batteries of composite solid-state electrolytes prepared by adding different fillers (NZSPO, Al_2O_3, SiO_2) to PPD materials (0.2 mA/cm^2, 0.2 mAh/cm^2).

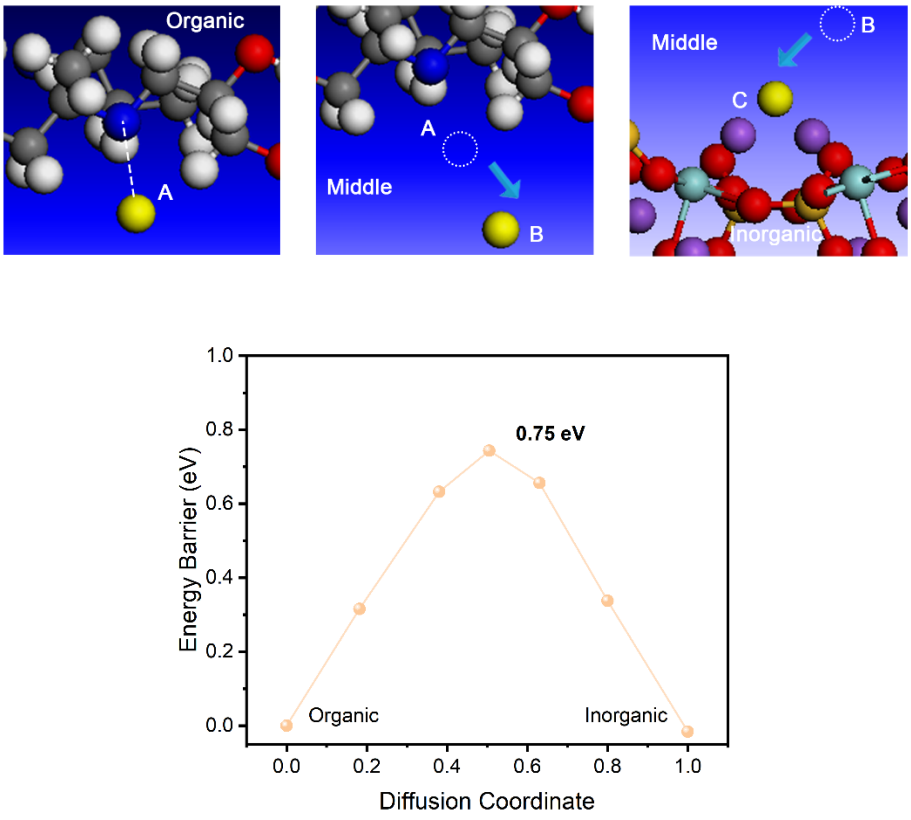

Fig. S11 A schematic diagram of the path of Na's migration from organic substances to inorganic substances and its migration energy barrier

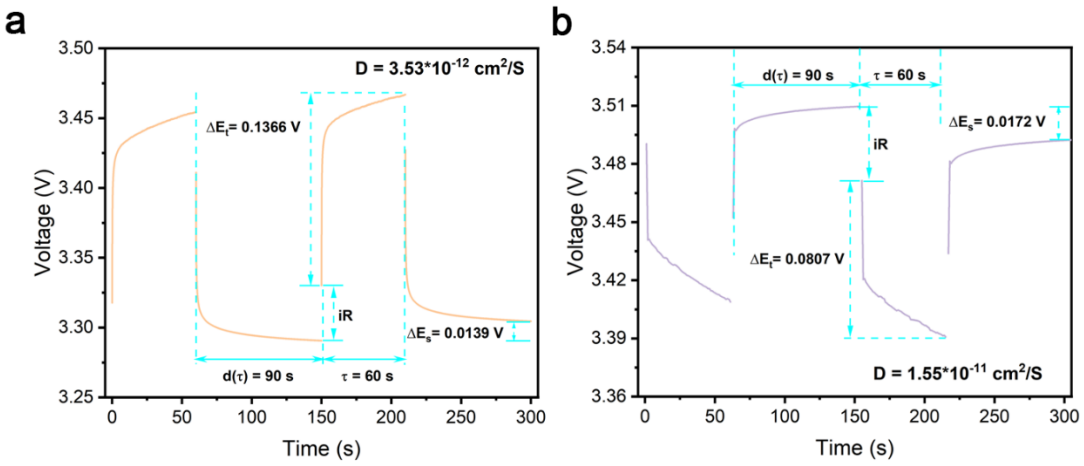

Fig. S12 The charge a) and discharge b) relaxation curves of the full battery assembled with PPD-0 in some voltage ranges.

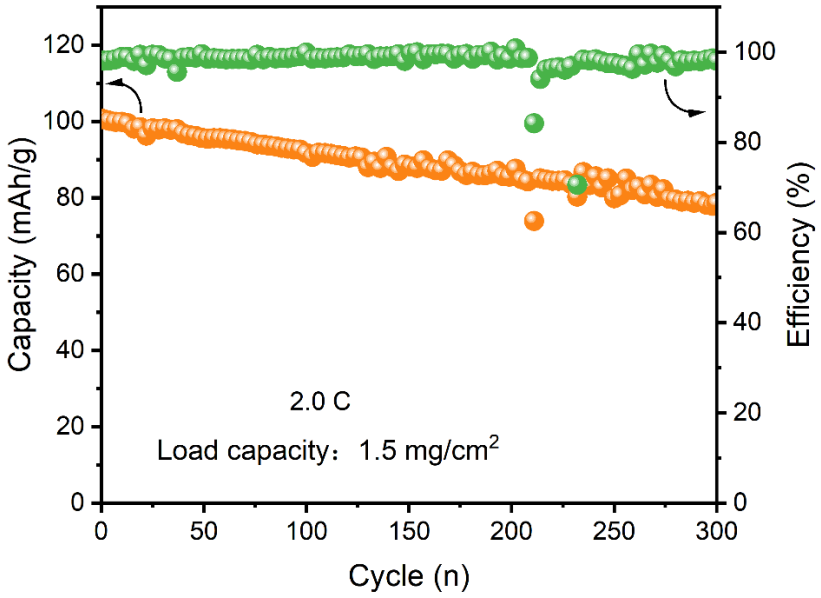

Fig. S13 Cycling performances of Na | PPD-10 | NVP batteries at 2.0C (loading conditions: 1.5 mg/cm^2).

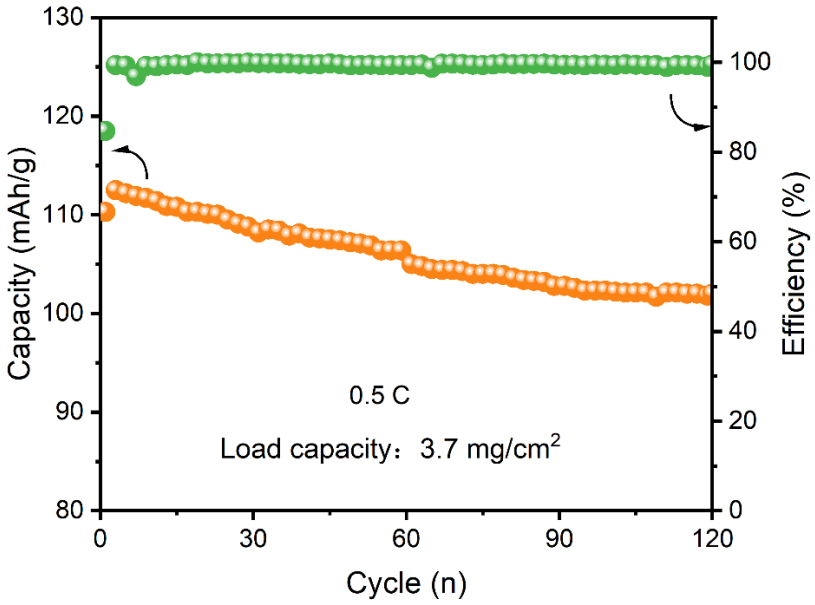

Fig. S14 Cycling performances of Na | PPD-10 | NVP batteries at 0.5C (loading conditions: 3.7 mg/cm^2).

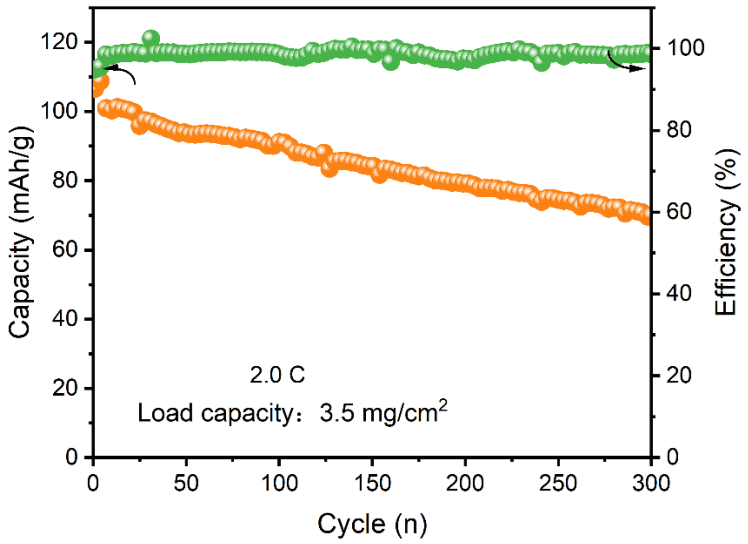

Fig. S15 Cycling performances of Na | PPD-10 | NVP batteries at 2.0C (loading conditions: 3.5 mg/cm^2).

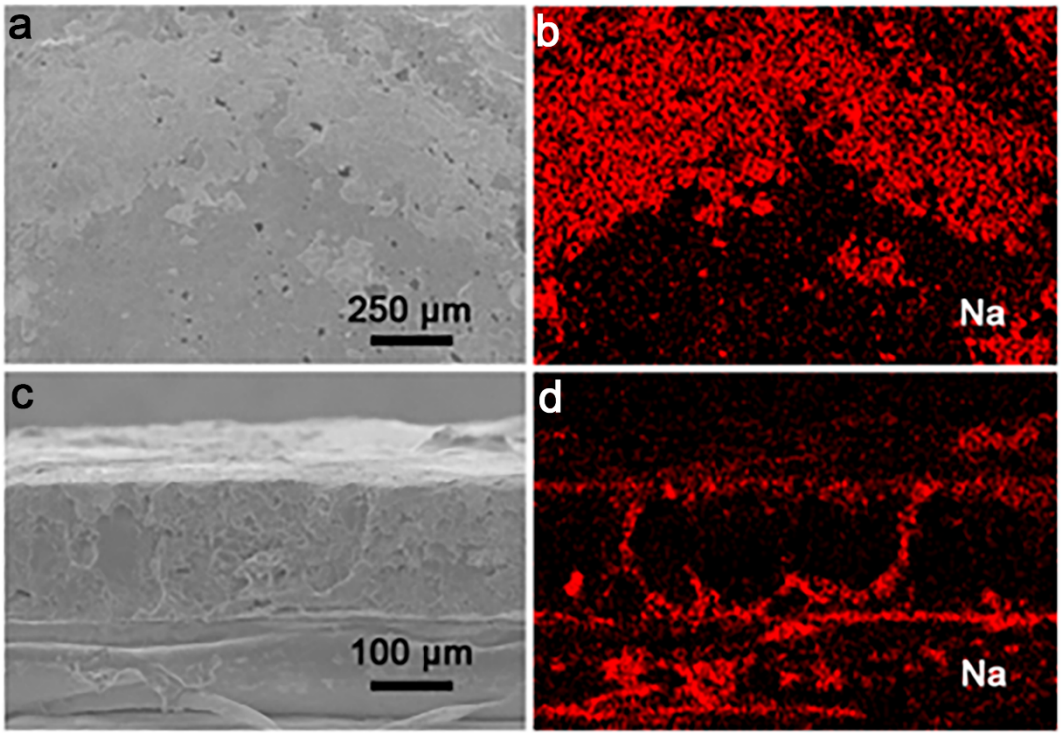

Fig. S16 The a) SEM image and b) elemental mapping photos of the PPD-0 surface after cycles; The c) SEM and d) elemental mapping photos of the PPD-0 in the cross-section view after cycles.

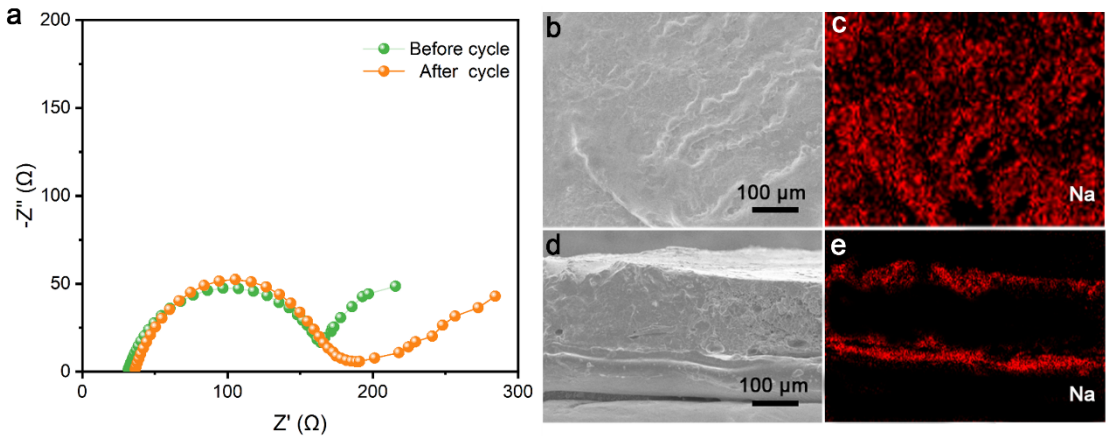

Fig. S17 a) The electrochemical impedance spectroscopy (EIS) curves of the full battery assembled with PPD-10 before and after the cycling process. The b) SEM and c) elemental mapping photos of the PPD-10 surface after cycles; The d) SEM and e) elemental mapping photos of the PPD-10 in the cross-section view after cycles.

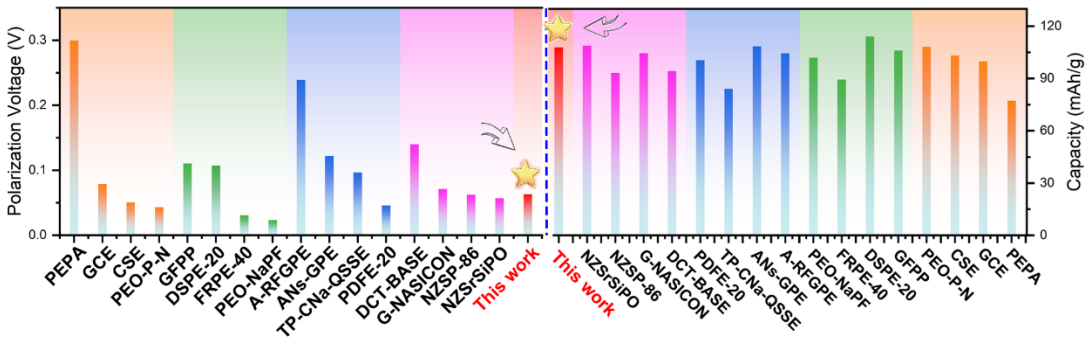

Fig. S18 Comparison of polarization voltage and capacity of this work and previous reported works assembled with electrolyte materials of different types.

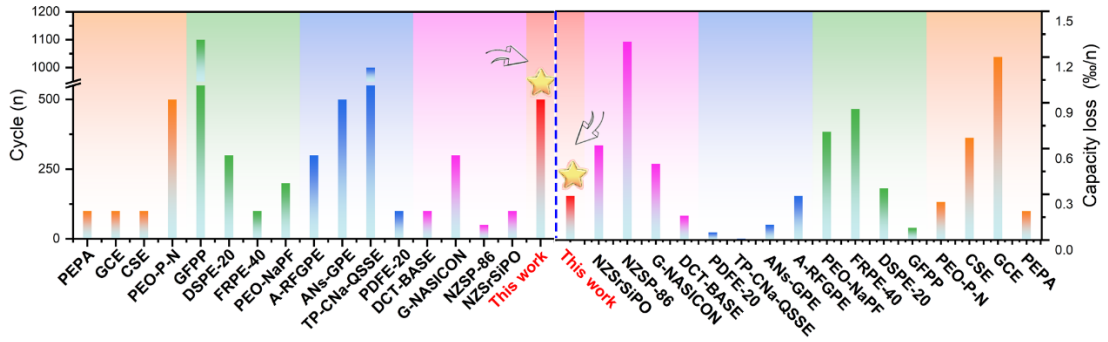

Fig. S19 Comparison of the cycle numbers and capacity loss of full batteries of this work and previous reported works assembled with electrolyte materials of different types.

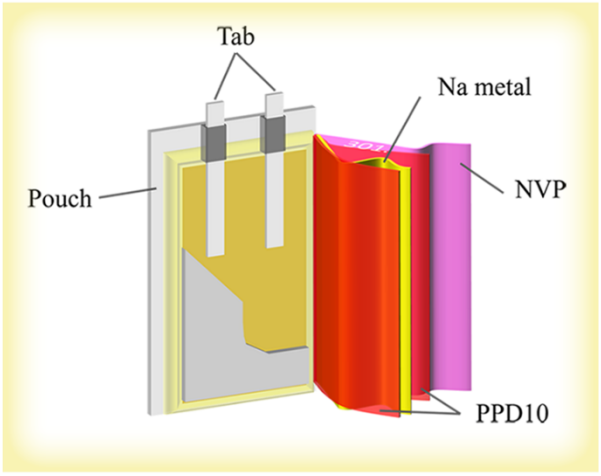

Fig. S20 Schematic diagram of pouch cell with NVP as cathode, Na metal as anode, and PPD-10 as solid-state electrolyte.

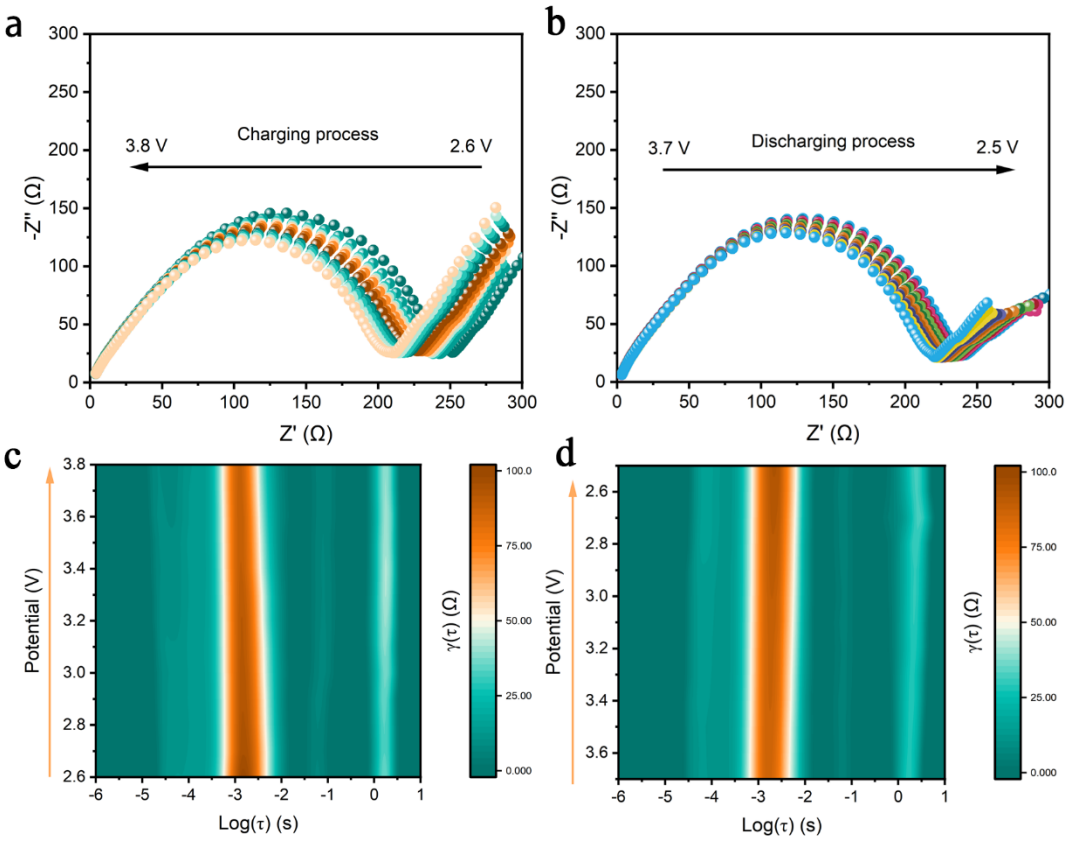

Fig. S21 In-situ EIS testing and Distribution of Relaxation Times (DRT) analysis of the Na/PPD-10/NVP all-cell battery.

Table S1. Electrochemical Performance of various types of batteries.

Inorganic electrolyte							
Electrolyte	Current intensity (mA cm^{-2})	Stable time (h)	Capacity (mAh g^{-1})	Polarization (V)	Cycle number	Lap loss (‰)	Reference
This work	0.2	2500	107.8	0.063	500	0.29	-
BASE	0.1	200	100.6	0.14	100	0.16	[1]
NZSP-3BTO	0.1	1000	-	-	-	-	[2]
CPE	0.2	1125	-	-	-	-	[3]
NZSP-0.2Cu	0.2	1450	-	-	-	-	[4]
Na_3BS_3	0.013	2500	-	-	-	-	[5]
G-NASICON	-	-	106	0.071	300	0.5	[6]
NZSP-86	-	-	78	0.063	50	1.3	[7]
NZSrSiPO	-	-	110.2	0.056	100	0.62	[8]
Polymer electrolyte							
NaFNFSI/PEO	0.1	200	-	-	-	-	[9]
FRPE-40	0.1	500	84.9	0.031	100	0.86	[10]
EO10-PFPE	0.1	780	-	-	-	-	[11]
PEGDMA-NaFSI	0.1	800	-	-	-	-	[12]
DSPE-20	0.1	1000	109	0.108	300	0.34	[13]
GFPP	-	-	105	0.11	1100	0.08	[14]
PEO-NaPF	-	-	93.8	0.104	200	0.71	[15]
Gel electrolyte							
ANs-GPE	0.5	300	99.5	0.27	300	0.16	[16]
GPE	0.5	400	-	-	-	-	[17]
PDFE-20	0.5	500	104	0.168	100	0.29	[18]
PSB60-GPE	0.5	800	-	-	-	-	[19]
A-FRGPE	0.1	950	102.6	0.24	300	0	[20]
TP-CNa-QSSE	-	-	87.7	0.098	1000	0.05	[21]
Composite electrolyte							
PEPA	0.1	390	93.6	0.3	100	0.19	[22]
GCE	0.2	600	95	0.079	100	1.2	[23]
ATFPE	0.05	620	-	-	-	-	[24]
SCE	0.1	1000	-	-	-	-	[25]
PEO-P-N	0.1	1000	102	0.043	500	0.25	[26]
CSE	-	-	106	0.05	100	0.67	[27]

Reference:

[1] X. Chi, F. Hao, J. Zhang, X. Wu, Y. Zhang, S. Gheytani, Z. Wen, Y. Yao, *Nano Energy*, 2019, **62**, 718-724.

[2] Z. Sun, Y. Zhao, Q. Ni, Y. Liu, C. Sun, J. Li, H. Jin, *Small*, 2022, **18**, 2200716.

[3] S. Bag, C. T. Zhou, S. Reid, S. Butler, V. Thangadurai, *J. Power Sources*, 2020, **454**, 227954.

[4] D. Li, C. Sun, C. Wang, J. Li, Z. Wang, H. Jin, *Energy Storage Mater.*, 2023, **54**, 403-409.

[5] A. Nasu, T. Inaoka, F. Tsuji, K. Motohashi, A. Sakuda, M. Tatsumisago, A. Hayashi, *ACS Appl. Mater. Interfaces*, 2022, **14**, 24480-24485.

[6] E. Matios, H. Wang, C. Wang, X. Hu, X. Lu, J. Luo, W. Li, *ACS Appl. Mater. Interfaces*, 2019, **11**, 5064-5072.

[7] J. A. S. Oh, X. Xu, Z. Zeng, K. Wang, N. Y. J. Tan, E. Kok, J. Huang, L. Lu, *Energy Environ. Mater.*, 2023, **6**, e12472.

[8] Q. Wang, C. Yu, L. Li, X. Liu, X. Zhang, G. Gao, Y. Wang, G. Li, *Energy Storage Mater.*, 2023, **54**, 135-145.

[9] Q. Ma, J. Liu, X. Qi, X. Rong, Y. Shao, W. Feng, J. Nie, Y.-S. Hu, H. Li, X. Huang, L. Chen, Z. Zhou, *J. Mater. Chem. A*, 2017, **5**, 7738-7743.

[10] B. Zhou, C. Yang, F. Wu, T. Deng, S. Guo, G. Zhu, Y. Jiang, Z. Wang, *Chem. Eng. J.*, 2022, **450**, 138385.

[11] X. Wang, C. Zhang, M. Sawczyk, J. Sun, Q. Yuan, F. Chen, T. C. Mendes, P. C. Howlett, C. Fu, Y. Wang, X. Tan, D. J. Searles, P. Král, C. J. Hawker, A. K. Whittaker, M. Forsyth, *Nat. Mater.*, 2022, **21**, 1057-1065.

[12] Y. Yao, Z. Wei, H. Wang, H. Huang, Y. Jiang, X. Wu, X. Yao, Z. S. Wu, Y. Yu, *Adv. Energy Mater.*, 2020, **10**, 1903698.

[13] H. M. Law, J. Yu, S. C. T. Kwok, G. Zhou, M. J. Robson, J. Wu, F. Ciucci, *Energy Storage Mater.*, 2022, **46**, 182-191.

[14] C. Luo, Q. Li, D. Shen, R. Zheng, D. Huang, Y. Chen, *Energy Storage Mater.*, 2021, **43**, 463-470.

[15] Q. Zhang, Y. Lu, H. Yu, G. Yang, Q. Liu, Z. Wang, L. Chen, Y.-S. Hu, *J. Electrochem. Soc.*, 2020, **167**, 070523.

[16] D. Lei, Y.-B. He, H. Huang, Y. Yuan, G. Zhong, Q. Zhao, X. Hao, D. Zhang, C. Lai, S. Zhang, J. Ma, Y. Wei, Q. Yu, W. Lv, Y. Yu, B. Li, Q.-H. Yang, Y. Yang, J. Lu, F. Kang, *Nat. Commun.*, 2019, **10**, 4244.

[17] Y. N. Zhou, Z. Xiao, D. Han, L. Yang, J. Zhang, W. Tang, C. Shu, C. Peng, D. Zhou, *Adv. Funct. Mater.*, 2022, **32**, 2111314.

[18] J. Ma, X. Feng, Y. Wu, Y. Wang, P. Liu, K. Shang, H. Jiang, X. Hou, D. Mitlin, H. Xiang, *J. Energy Chem.*, 2023, **77**, 290-299.

[19] H. Lai, Y. Lu, W. Zha, Y. Hu, Y. Zhang, X. Wu, Z. Wen, *Energy Storage Mater.*, 2023, **54**, 478-487.

[20] M. Yang, F. Feng, Z. Shi, J. Guo, R. Wang, Z. Xu, Z. Liu, T. Cai, Z. Wang, C. Wang, S. Chen, Z.-F. Ma, T. Liu, *Energy Storage Mater.*, 2023, **56**, 611-620.

[21] Y. Yan, Z. Liu, T. Wan, W. Li, Z. Qiu, C. Chi, C. Huangfu, G. Wang, B. Qi, Y.

Yan, T. Wei, Z. Fan, *Nat. Commun.*, 2023, **14**, 3066.
[22] T. Y. Wang, M. Zhang, K. F. Zhou, H. L. Wang, A. H. Shao, L. Y. Hou, Z. Q. Wang, X. Y. Tang, M. Bai, S. W. Li, Y. Ma, *Adv. Funct. Mater.*, 2023, **33**, 2215117.
[23] L. Ran, S. Tao, I. Gentle, B. Luo, M. Li, M. Rana, L. Wang, R. Knibbe, *ACS Appl. Mater. Interfaces*, 2021, **13**, 39355-39362.
[24] J. Guo, F. Feng, S. Zhao, R. Wang, M. Yang, Z. Shi, Y. Ren, Z. Ma, S. Chen, T. Liu, *Small*, 2023, **19**, 2206740.
[25] L. Ran, M. Li, E. Cooper, B. Luo, I. Gentle, L. Wang, R. Knibbe, *Energy Storage Mater.*, 2021, **41**, 8-13.
[26] E. Matios, H. Wang, J. Luo, Y. Zhang, C. Wang, X. Lu, X. Hu, Y. Xu, W. Li, *J. Mater. Chem. A*, 2021, **9**, 18632-18643.
[27] J. F. Wu, Z. Y. Yu, Q. Wang, X. Guo, *Energy Storage Mater.*, 2020, **24**, 467-471.